Radon Transport from Soil to Air and Monte-Carlo Simulation

Ahmad Muhammad
Firat University
Fatih Külahcı (fatihkulahci@firat.edu.tr)
Firat University

Research Article

Keywords: Radon transport, soil-air migration, Monte Carlo Simulation, Seismo-Ionospheric Coupling

Posted Date: November 30th, 2021

DOI: https://doi.org/10.21203/rs.3.rs-1088944/v1

Version of Record: A version of this preprint was published at Journal of Atmospheric and Solar-Terrestrial Physics on November 1st, 2021. See the published version at https://doi.org/10.1016/j.jastp.2021.105803.

Radon Transport from Soil to Air and Monte-Carlo Simulation

Ahmad Muhammad, Fatih Külahcı*

Fırat University, Faculty of Science, Department of Physics, Nuclear Physics Division, TR-23119, Harput, Elazig, Turkiye

*Corresponding author. Tel: +90 424 2370000/3835; Fax: +90 424 2330062; Email: ahmadmuhammad325@gmail.com, fatihkulahci@firat.edu.tr

Abstract

The exhalation of geochemical entities from soil to air is significant to understand Lithosphere-Atmospheric relationships. Some of these geochemical entities are capable of modifying the lower atmosphere, and they are employed in various studies. Radon is one of the geochemical gasses widely recognized as a dominant ionization source in near ground regions of the troposphere. The steady state Rn transport equation is considered in many cases for estimating Rn migration from soil to air on the condition that the time evolution is ignored. A method is proposed for estimating radon space-time transport from soil to air. This is achieved by solving the radon transport equation in soil with special boundary conditions. Similar results are obtained with some experimented models, as well as reported radon values in literature for some set of parameter combinations. Strengths and limitations of the method are discussed. The model is useable to study Lithosphere-Atmosphere relationships. It can also be significant in other studies like the Global Electric Circuit or Seismo-Ionospheric studies.

Keywords: Radon transport; soil-air migration; Monte Carlo Simulation; Seismo-Ionospheric Coupling

1.0 Introduction

Radon is one of the natural gasses constantly exhaled into the atmosphere from the soil. ^{222}Rn is the most prominent radon isotope, which is able to find its way through soil pore channels into the atmosphere or buildings without reacting with any atom in the process. Its density, radioactive property, and ubiquity are the reason why it is exploited in a variety of applications. For example, it is used as a hydrological tracer, its accumulation in a given aquifer is helpful to estimate the aquifer residence time (Grunwald, 2004). Radon distribution in a given region helps to locate subsurface uranium and hydrocarbon deposits (Baskaran, 2016; Grunwald, 2004). Soil and water Rn anomalies are well known in earthquake precursory studies (Ali et al., 2019), its concentration can increase (Erees et al., 2007) or decrease (Omori et al., 2007) in relation to seismic activities. It is used as atmospheric tracer in the study of atmospheric transport processes, selection of least-perturbed marine air masses for baseline studies, tracing of terrestrial air mass movements, including the refinement of source footprints for aerosols in continental outflow events, calibration of regionally integrated emissions of important greenhouse gases, electric field studies, understanding pollutant concentrations behavior, and quantification of vertical mixing in the lower atmosphere (Williams et al., 2011). As such, Rn has received attention from researchers since several decades, and statistical and modeling studies are published worldwide. Rn exhalation can vary depending on the geology, geochemistry, as well as soil properties of a given region (Külahcı and Şen, 2014; Warden et al., 2019). This exhalation is often associated with gasses like methane, carbon dioxide, hydrogen, and helium. Rn exhalation can be affected by soil and atmospheric processes, like metrological, geological, as well as other physical factors (Külahcı and Şen, 2014; Victor et al., 2019). This makes it important in studying the relationships between lithosphere and atmospheric processes. Its ability to ionize the environment makes it play an important role in tropospheric electricity studies. Moreover, its decay chain includes short-lived radio-isotopes (Polonium and Bismuth), which are charged, and capable of irradiating aerosol particles, while attached to them, and this can lead to effects which may result in disturbances in upper atmospheric heights (Namgaladze et al., 2018; Sorokin et al., 2020). Therefore, understanding radon dynamics in soil is very important to its application in near surface

atmospheric studies, especially the processes that can result in upper atmospheric perturbations. Rn transport in soil or air occurs mainly by diffusion or advection (Nazaroff, 1992), and the processes involved in this transport depend on the soil conditions. In literature, several theoretical and experimented models have been presented for soil radon (Catalano et al., 2015; Chakraverty et al., 2018; Orabi, 2018; Phong Thu et al., 2020; Singh et al., 2016) to mention a few. Some of these studies have considered transport models, which give a zero radon concentration at the surface. These models would give good outcomes if only soil radon distribution is a priority and the concentration at the surface is trivial. However, Antonopoulos-Domis et al. (2009) argued that this is not the best way to deal with the problem if there is the need to better estimate Rn concentration reaching the surface. Especially, since surface Rn concentration is one of the major sources for observed atmospheric Rn variations, as well as tropospheric ionization. Thus, these models may not favor studies, which seek to explore lithosphere-atmosphere relationships. Other Rn studies in literature are established only based on radon time series variability (Hayashi et al., 2015; Kamişlioğlu and Külahci, 2016; Muhammad et al., 2021). One rarely finds a space-time dependent radon model, capable of estimating seasonal/diurnal, as well as spatial radon time series variability using historical data. The existence of such models would favor Seismo-Ionospheric coupling studies, especially regarding radon ionization capability.

In this study, a novel method is proposed for estimation of surface radon concentration using recorded soil radon data at a given depth. The resulting equation from the method can be used to study radon surface variations, soil radon distribution under different production rates as well as radon space-time variability at any depth in soil. In Section 2, the soil to air radon transport model is presented and the model parameters are discussed. In Section 3, model outcomes are compared with literature. Additionally, the surface radon is estimated and discussed for Eksisu monitoring station, Erzincan, a city along the North Anatolian Fault Zone (NAFZ), Turkiye. Finally, Monte Carlo method is applied to simulate the estimated surface radon concentration to account for estimation uncertainties.

2.0 Proposed method

2.1 Radon transport equation

The recorded radon concentration at monitoring depth may generate radon impulse exported from neighboring or far regions added to the radon production in the vicinity of the monitoring device. The study of these relationships is significant in the establishment of soil radon migration relation, and can be used to explain its transport from the production point to the atmosphere. Radon transport is generally represented by the space-time convective-diffusive equation. The 1D soil radon transport equation reads (Nazaroff, 1992; Antonopoulos-Domis et al., 2009; Muhammad et al., 2020):

$$\frac{\partial C_{Rn}}{\partial t} = D\frac{\partial^2 C_{Rn}}{\partial z^2} - u\frac{\partial\, C_{Rn}}{\partial z} - \lambda C_{Rn} + F \tag{1}$$

where C_{Rn} (kBqm^{-3}) is the generated/recorded radon concentration in soil pore air channels of the monitoring depth, D (m^{2}s^{-1}) is the effective radon diffusion coefficient in soil, u (ms^{-1}) is the effective advective radon velocity in soil, λ is radon decay constant $2.1\times10^{6}s^{-1}$, and F is the rate at which radon atoms are produced. F is defined in terms of the soil bulk density ρ, the soil Radium (^{226}Ra) concentration C_{Ra} (Bqm^{-3}), the soil radon emanation coefficient ε, and the radon decay constant λ (Nazaroff, 1992).

$$F = \lambda\varepsilon C_{Rn}\rho \tag{2}$$

Assuming that the recorded radon concentration at a depth z by the monitoring device is produced by atoms in its locality, and that the vertical transport of radon dominates compared to its transport in other directions, if one places the origin of z-axis on the Earth's surface and positive downwards, the boundary conditions suitable for simulation of Eqn. (1) can be written in the following form:

$$C_{Rn}(0,t) = f(t)(1-\alpha),\ \left.\frac{\partial C_{Rn}(z,t)}{\partial z}\right|_{z\to\infty} = 0 \tag{3}$$

Herein, $f(t)$ is the recorded radon concentration at the monitoring depth. It can also be expressed as a function or a model, which represents the radon time series variation at any given time t at the radon monitoring depth z, where α is the attenuation coefficient. It represents the fraction of radon concentration lost in its journey to the crustal surface. The boundary conditions in Eqn (3), are the only significant improvements in solving the radon transport equation (Eqn (1)), and the estimation can be done in a variety of ways, depending on the problem at hand. The boundary conditions employed here assume that radon concentration decreases by α upon reaching the soil

from production depth beneath the soil, and there is enough radium content such that the spatial concentration does not change over time. Eqn. (1) can be solved using separation of variables, and its general solution alongside the boundary conditions in Eqn. (3) is given by:

$$C_{Rn}(z,t) = Q(1-\exp(-az)) + f(t)(1-\alpha)\exp(-az) \quad (4)$$

based on $a = -\frac{u}{2D} + \sqrt{\frac{u^2}{4D^2} - \frac{(w-\lambda)}{D}}$, where w is the time evolution constant (s^{-1}), which controls the rate of radon per unit time change , and $Q = \frac{F}{\lambda}$ represents radon concentration at a distance further from the monitoring depth. If Q is far away from the monitoring depth $f(t)$, and the geology of the monitoring region is such that radon concentration increases with depth, then Q represents the radon concentration in secular equilibrium with soil radium content at a given depth, and hence, all discussions are centralized around Eqn. (4).

2.2 Model parameters

Eqn. (4) is flexible in its application to estimate soil radon space-time vertical distribution. The major parameters required to estimate radon at a depth *z* at a given time *t* are $f(t)$, α Q, and a, furthermore there are two ways for the application of $f(t)$ in the same equation. First, the Rn concentration values are applicable directly provided that the parameters, Q, and α are known in the monitoring region. Secondly, $f(t)$ can be established as a function to represent soil radon variation with minimum error. The parameter α takes the values between 0 and 1 as the fraction, which the recorded Rn concentration generation at a depth *z* is reduced reaching the surface. If $\alpha = 0.9$ then about 90% of $f(t)$ is lost during radon migration from production point to the surface. On the other hand, α is best applicable to Eqn. (4) in cases where the measured radon concentration at some depth *z* is comparable with radon concentration at the surface. For example, Almayahi et al. (2013) reported surface radon concentration in the Northern Peninsular, Malaysia to vary between 6 Bqm^{-3} and 79 Bqm^{-3}, and these correspond to 133 Bqm^{-3} and 143059 Bqm^{-3} at 50 cm depth. Comparing this observation with the proposed method, Eqn. (4) estimates a surface concentration of 6 Bqm^{-3} and 79 Bqm^{-3}, respectively for the measured 133 Bqm^{-3} and 143059 Bqm^{-3} at the same 50 cm depth, this is achieved with , $\alpha = 0.954323$ & $\alpha = 0.999444$. The parameter, $Q = \varepsilon C_{Rn} \rho$ is obtainable by directly using the independent variables in its equation, or by directly

measuring radon concentration at a depth further than the monitoring depth, or can be left as regression coefficient to be determined by the least square fitting method. The last parameter a can be determined in similar way.

3.0 Model estimations

3.1 Radon soil distribution

Eqn. (4) helps to estimate radon concentration reaching the surface $z = 0$ in different ways. However, in most cases, data availability plays significant role in the problem approach. Two methods exist to illustrate the flexibility of applying the equation, namely comparison of the model outcomes to that of Antonopoulos-Domis et al. (2009), and application of the model to estimate recorded radon at a 1m depth. As for Antonopoulos-Domis et al. (2009), they established a steady state soil radon profile model using a decent surface boundary condition, given by:

$$C_{Rn}(z) = I_{\infty}\left(1 - \frac{\exp(-az)}{1 + a/k}\right) \qquad (5)$$

where I_{∞} is the concentration at depths for relatively uniform radon distribution , it is equivalent to Q in Eqn. (4), and the parameter a in Eqn. (5) is similar to that in Eqn. (4) if w is set to zero. Furthermore, k is proportionality constant for radon transport control at soil-air boundary. At depths where Radon concentration is relatively constant, $f(t) \approx Q$, and Eqn. (4) approximates to Eqn. (5) yielding exactly the same outcomes with $\alpha = \frac{1}{1 + a/k}$. To illustrate this, soil radon profile simulation is implemented using Eqn. (5) for $I_{\infty} = 20 kBqm^{-3}$ and the parameter combination $k = 186, a = 0.905$, at a depth 0 to 1 meter (red curve in Figure 1A). Eqn. (4) is simulated assuming that the monitoring device is located, where the radon is in secular equilibrium with its mother nuclide $f(t) \approx Q \approx 20 kBqm^{-3}$ (blue dashed curve in Figure 1A). However, in some cases, radon concentration at the monitoring depth can be greater or less compared to that at further depths within the soil. This may occur due to localized soil inhomogeneity or spatial gradients in soil Radium/Uranium content or even when radon measurements are recorded at shallow depths (e.g. $z < 1m$). This would limit Eqn. (5) to approximate a single concentration influence, while Eqn. (4) could account for such localized changes. Let $Q > f(t)$, such that $Q = 25 kBqm^{-3}$ and $f(t) = 20 kBqm^{-3}$, as shown in Figure 1B or the case, where $Q < f(t)$, such that $Q = 20 kBqm^{-3}$ $f(t) = 25 kBqm^{-3}$ (Figure 1C).

3.2 Radon transport from soil to air

As demonstrated in section 3.1, soil properties can influence the model outcome of Eqn. (4). The choice of parameter combination is very important and experiments need to be conducted in order to determine the parameter combinations suitable for different geological regions. In most cases, radon concentration at a given depth z (i.e. $f(t)$) is the only readily available parameter, while Q, a, and α are scarcely available. In this case, assumptions are needed before implementing the model, and this depends on the type of problem at hand. To illustrate this, one can apply Eqn (4) to estimate surface radon concentration from soil radon data collected from Eksisu, Erzincan, a city along the NAFZ, Turkiye.

3.2.1 Data collection

Rn concentration is recorded at 15 minutes' interval. AlphaMeter 611 sensors manufactured by AlphaNuclear Co. (Canada) are used for the continuous monitoring. The AlphaMeter 611 sensors are installed at a shallow borehole (≈ 1 m) and covered by soil. The data collection system automatically stores the data in a repository. This data is made available by the Ministry of Interior Disaster and Emergency Management Presidency, Turkiye (AFAD, https://en.afad.gov.tr/).

3.2.2 Radon estimation

Assuming the need to estimate the daily mean surface radon concentration at Eksisu monitoring station, say from 12th April to 19th July 2008 (Figure 2). It is necessary to first identify $f(t)$. Due to the seasonal behavior of radon along fault regions (Font et al., 2008; Miklyaev et al., 2020; Muhammad et al., 2020; Siino et al., 2019), herein $f(t)$ is defined as a Fourier series function such that (Danbatta and Varol, 2021):

$$f(t) = \sum_n A_n Cos(nwt) + B_n Sin(nwt) \tag{6}$$

where $w = \frac{2\pi}{T}$ is the radon seasonal frequency, $T = 365.5$ days, n is the order of the Fourier series function, and the coefficients A_n & B_n are determined by least square fitting method. Order of $n = 9$ is chosen as the Fourier function, which best describes the soil radon data. A linear relationship exists between soil Rn and the Fourier function (see Figure 3A). The model could account for

about 99% of radon soil variation with a root mean square error of about 1.5, and its residual fits the theoretical normal (Gaussian) probability distribution function (Figure 3B). Such high model accuracy can result in poor forecast performance (Adhikari and Agrawal, 2013). However, the aim is not to forecast, but to enable the generation of multiple values for each radon prediction by the model accounting for uncertainty in predicted radon concentrations.

The second important parameter is Q, which can help in understanding the relationship between radon production and the recorded radon at a given depth z. Herein, a case is considered, where the recorded radon $f(t)$ is almost similar to the produced radon concentration at greater depths. As for the latter, since the Eksisu Rn is monitored at 1m depth, and there exists a possibility of higher radon concentrations at 1.5 or 2m depths (Antonopoulos-Domis et al., 2009; Orabi, 2018; Várhegyi et al., 2013). In line with this, depending on the choice of reference, Q can assume any value higher than $f(t)$ since the radon monitoring device is not located at depths where $\left.\frac{\partial C_{Rn}(z,t)}{\partial z}\right|_{z\to\infty} = 0$. Thus, herein the case is considered, where $Q_i \approx f(t_i)+\sigma$ represents Q for any given observation $f(t_i)$. Herein, $i = (0, 1, 2, 3, \ldots)$ is the time count when the observations are recorded (with zero as the first recorded radon observation) and σ is the standard deviation of $f(t)$. The parameters α and a are chosen such that, Eqn. (4) is able to re-generate the recorded radon concentration at 1m depth as well as giving decent estimates for the surface variations.

In Figure 4, the estimated radon concentration is shown at 1m depth (Figure 4A), and at the surface (Figure 4B) with the soil to air distribution profile (Figure 4C). In Figures 4A and B, the blue dotted curves represent the estimated radon concentration for $Q_i \approx f(t)$, while the black solid curves represent radon concentrations for the case where $Q_i \approx f(t_i)+\sigma$. These estimations were achieved with $\alpha \approx 0.99$, and $a \approx 5$. The statistical properties of these estimations are presented in Table 1. In Figure 4A, a decent radon estimation is observed for the case, where $Q_i \approx f(t)$, whereas, $Q_i \approx f(t_i)+\sigma$ estimates higher values, which means that if the flow of radon produced at the locality (or at further depths) of the monitoring device is not in equilibrium to that which is recorded at the monitoring depth, then $f(t)$ will be affected in a similar way by the production rate. This effect can be significant, especially, in the study of seismically induced radon variations, where crustal movements cause abnormal radon variabilities (e.g. in (Garcìa et al., 2000; Koike et

al., 2014)). Regardless of Q, the radon concentration reaching the surface approaches the values recorded by atmospheric radon sensors. The surface radon at Eksisu monitoring station is presented in Figure 4B, and the last two rows of Table 1. The estimated surface radon varies between 35 to 293Bqm^{-3}, with mean and standard deviation values as 134Bqm^{-3} and 77Bqm^{-3}, respectively (Table 1).

Table 1 Statistical properties of estimated results.

ALL IN UNITS OF Bqm^{-3}	**MEAN**	**STD**	**MIN**	**25%**	**50%**	**75%**	**MAX**
RADON	29285.9	17038.32	7375.000	16072.92	23864.58	39203.13	65583.58
FOURIER ORDER-9 $f(t_i),\ z=1$	29285.9	16972.95	7823.095	16114.16	22802.62	39665.85	64016.64
SOIL RADON $Q_i = f(t_i),\ z=1$	29089.5	16859.11	7770.625	16006.08	22649.68	39399.81	63587.27
SOIL RADON $Q_i = f(t_i)+\sigma,\ z=1$	45859.12	16859.11	24540.25	32775.71	39419.30	56169.44	80356.89
SURFACE RADON $Q_i = f(t_i)+\sigma,\ z=0$	134.2174	77.78703	35.85325	73.85121	104.5044	181.7886	293.3882
SURFACE RADON $Q_i = f(t_i),\ z=0$	134.2174	77.78703	35.85325	73.85121	104.5044	181.7886	293.3882

These surface values are acceptable as the estimation is done near an active fault region, and radon can have higher values in such regions (Miklyaev et al., 2020; Muhammad et al., 2021). Moreover, April to July are months having less soil moisture content (summer), meaning that the exhalation rate is favored due to enhanced porosity. There is not available data to compare with the model outcomes, therefore, 99 multiple paths for the estimated radon are simulated using Monte Carlo method (Figure 5). This method is similar to that of (Muhammad et al., 2020). The difference is that, the paths are generated within $\pm RMSE$ of the Fourier model curve. This is done because radon concentration is affected, while being transported through soil pore channels. For example, it can be affected by meteorological factors (temperature or pressure gradients), as well as geological factors (e.g. entrapment in some soil dense region). The generated paths hopefully cover these and other possible uncertainties associated with the estimated surface radon values.

3.3 Method Limitations and Applications

One of the limitations of Eqn. (4) is the need to have radon values in soil and at the surface, or at least in soil, in order to achieve decent estimation results. In addition, the model in its current form does not have the capability to explicitly account for meteorological or other physical effects on radon transport (e.g. the approach by (Chuan Chen et al., 1995)). In order to study such changes,

there is the need to improvise (e.g. using statistical approach). Moreover, the equation needs experimental implementation in order to determine the best value for each parameter in different soil conditions.

On the other hand, this method is significant to study the processes occurring between soil and Earth's atmosphere. It can also be significant in modeling relationship between radon, earthquake, and ionosphere. This is because radon and its progeny are capable of ionizing their surroundings, and then Eqn. (4) can be used to study the ions generation movement, and charged aerosols from soil to the atmosphere. This is very important, especially in understanding; Seismo-Ionospheric coupling processes (Ampferer et al., 2010; Denisenko, 2015; Kuo et al., 2014; Namgaladze et al., 2018; Sorokin et al., 2020).

3.0 Conclusions

The soil migration mechanism for Radon can be studied via solving the transport equation in soil with special boundary conditions. A method for estimation of surface radon concentration using recorded soil radon data at a given depth is presented. The resulting equation from the method was used to study radon surface variations. It can also be applied to study soil radon distribution under different production rates as well as radon space-time variability at any depth in soil. Similar results are obtained with some experimented models (as well as observations) in the literature for some set of parameter combinations. This approach can be suitable in studying Lithosphere-Atmosphere relationships; it can also be significant in other studies like the Seismo-Ionospheric studies. The surface Rn concentration is predicted by using the amount of Rn gas at a given depth. With this method, not only the surface Rn concentration, but also spatial surface variations of Rn can be applied to determine the space-time variations of Rn in soil. Finally, since Radon concentration can vary depending on geological settings, it is highly recommended to test robustness of the method, especially in heterogeneous environments.

Acknowledgments

We would like to thank Disaster and Emergency Management Presidency, (https://en.afad.gov.tr/) for Rn data. This research was carried out as part of Ahmad Muhammad's PhD Thesis. The authors thank the Fırat University for supporting this study and other PhD thesis study "Muhammad, A., et al 2021. J. Atmos. Solar-Terrestrial Phys. 221, 105688. https://doi.org/10.1016/j.jastp.2021.105688" and preparing a suitable study environment.

References

Adhikari, R., Agrawal, R.K., 2013. An Introductory Study on Time Series Modeling and Forecasting. arXiv Prepr. arXiv1302.6613 1302.6613, 1–68.

Ali, F.S.A., Mahdi, K.H., Jawad, E.A., 2019. Humidity effect on diffusion and length coefficient of radon in soil and building materials, in: Energy Procedia. Elsevier Ltd, pp. 384–392. https://doi.org/10.1016/j.egypro.2018.11.203

Almayahi, B.A., Tajuddin, A.A., Jaafar, M.S., 2013. In situ soil 222Rn and 220Rn and their relationship with meteorological parameters in tropical Northern Peninsular Malaysia. Radiat. Phys. Chem. 90, 11–20. https://doi.org/10.1016/j.radphyschem.2013.04.028

Ampferer, M., Denisenko, V. V, Hausleitner, W., Krauss, S., Stangl, G., Boudjada, M.Y., Biernat, H.K., 2010. Decrease of the electric field penetration into the ionosphere due to low conductivity at the near ground atmospheric layer. Ann. Geophys. 28, 779–787. https://doi.org/10.5194/angeo-28-779-2010

Antonopoulos-Domis, M., Xanthos, S., Clouvas, A., Alifrangis, D., 2009. Experimental and theoretical study of radon distribution in soil. Health Phys. 97, 322–331. https://doi.org/10.1097/HP.0b013e3181adc157

Baskaran, M., 2016. Radon: A Tracer for Geological, Geophysical and Geochemical Studies, Radon: A Tracer for Geological, Geophysical and Geochemical Studies. Springer International Publishing. https://doi.org/10.1007/978-3-319-21329-3

Catalano, R., Immé, G., Mangano, G., Morelli, D., Aranzulla, M., 2015. Radon transport: Laboratory and model study. Radiat. Prot. Dosimetry 164, 575–581. https://doi.org/10.1093/rpd/ncv314

Chakraverty, S., Sahoo, B.K., Rao, T.D., Karunakar, P., Sapra, B.K., 2018. Modelling uncertainties in the diffusion-advection equation for radon transport in soil using interval arithmetic. J. Environ. Radioact. 182, 165–171. https://doi.org/10.1016/j.jenvrad.2017.12.007

Chuan Chen, Thomas, D.M., Green, R.E., 1995. Modeling of radon transport in unsaturated soil. J. Geophys. Res. 100. https://doi.org/10.1029/95jb01290

Danbatta, S.J., Varol, A., 2021. Monte Carlo forecasting of time series data using Polynomial-Fourier series model. Int. J. Model. Simulation, Sci. Comput. 2141004. https://doi.org/10.1142/S179396232141004X

Denisenko, V. V, 2015. Estimate for the strength of the electric field penetrating from the Earth's surface to the ionosphere. Russ. J. Phys. Chem. B 9, 789–795. https://doi.org/10.1134/S199079311505019X

Erees, F.S., Aytas, S., Sac, M.M., Yener, G., Salk, M., 2007. Radon concentrations in thermal waters related to seismic events along faults in the Denizli Basin, Western Turkey. Radiat. Meas. 42, 80–86. https://doi.org/10.1016/j.radmeas.2006.06.003

Font, L., Baixeras, C., Moreno, V., Bach, J., 2008. Soil radon levels across the Amer fault. Radiat. Meas. 43, S319--S323. https://doi.org/10.1016/j.radmeas.2008.04.072

Garcìa, R., Natale, G., Monnin, M., Seidel, J.L., 2000. Shock wave radon surface signals associated with the upsurge of T-P solitons in volcanic systems. J. Volcanol. Geotherm. Res. 96, 15–24. https://doi.org/10.1016/S0377-0273(99)00141-9

Grunwald, E., 2004. Radon as tracer 5414–5420.

Hayashi, K., Yasuoka, Y., Nagahama, H., Muto, J., Ishikawa, T., Omori, Y., Suzuki, T., Homma, Y., Mukai, T., 2015. Normal seasonal variations for atmospheric radon concentration: A sinusoidal model. J. Environ. Radioact. 139, 149–153. https://doi.org/10.1016/j.jenvrad.2014.10.007

Kamışlıoğlu, M., Külahcı, F., 2016. Chaotic Behavior of Soil Radon Gas and Applications. Acta Geophys. 64, 1563–1592. https://doi.org/10.1515/acgeo-2016-0077

Koike, K., Yoshinaga, T., Ueyama, T., Asaue, H., 2014. Increased radon-222 in soil gas because of cumulative seismicity at active faults. Earth, Planets Sp. 66, 1–9. https://doi.org/10.1186/1880-5981-66-57

Külahcı, F., Şen, Z., 2014. On the Correction of Spatial and Statistical Uncertainties in Systematic Measurements of 222Rn for Earthquake Prediction. Surv. Geophys. 35, 449–478. https://doi.org/10.1007/s10712-013-9273-8

Kuo, C.L., Lee, L.C., Huba, J.D., 2014. An improved coupling model for the lithosphere-atmosphere-ionosphere system. J. Geophys. Res. Sp. Phys. 119, 3189–3205. https://doi.org/10.1002/2013JA019392

Miklyaev, P.S., Petrova, T.B., Marennyy, A.M., Shchitov, D. V, Sidyakin, P.A., Murzabekov, A., Lopatin, M.N., 2020. High seasonal variations of the radon exhalation from soil surface in the fault zones (Baikal and North Caucasus regions). J. Environ. Radioact. 219, 106271. https://doi.org/10.1016/j.jenvrad.2020.106271

Muhammad, A., Külahcı, F., Akram, P., 2020. Modeling radon time series on the North Anatolian Fault Zone, Turkiye: Fourier transforms and Monte Carlo simulations. Nat. Hazards 104, 979–996. https://doi.org/10.1007/s11069-020-04200-8

Muhammad, A., Külahcı, F., Salh, H., Hama Rashid, P.A., 2021. Long Short Term Memory networks (LSTM)-Monte-Carlo simulation of soil ionization using radon. J. Atmos. Solar-Terrestrial Phys. 221, 105688. https://doi.org/10.1016/j.jastp.2021.105688

Namgaladze, A., Karpov, M., Knyazeva, M., 2018. Aerosols and seismo-ionosphere coupling: A review. J. Atmos. Solar-Terrestrial Phys. 171, 83–93. https://doi.org/10.1016/j.jastp.2018.01.014

Nazaroff, W.W., 1992. Radon transport from soil to air. Rev. Geophys. 30, 137–160. https://doi.org/10.1029/92RG00055

Omori, Y., Yasuoka, Y., Nagahama, H., Kawada, Y., Ishikawa, T., Tokonami, S., Shinogi, M., 2007. Anomalous radon emanation linked to preseismic electromagnetic phenomena. Nat. Hazards Earth Syst. Sci. 7, 629–635. https://doi.org/10.5194/nhess-7-629-2007

Orabi, M., 2018. Multi-layer description model for radon concentration in soil. Eur. Phys. J. Plus 133. https://doi.org/10.1140/epjp/i2018-11967-2

Phong Thu, H.N., Van Thang, N., Hao, L.C., 2020. The effects of some soil characteristics on radon emanation and diffusion. J. Environ. Radioact. 216. https://doi.org/10.1016/j.jenvrad.2020.106189

Siino, M., Scudero, S., Cannelli, V., Piersanti, A., D'Alessandro, A., 2019. Multiple seasonality in soil radon time series. Sci. Rep. 9, 1–13. https://doi.org/10.1038/s41598-019-44875-z

Singh, P., Sahoo, B.K., Bajwa, B.S., 2016. Theoretical modeling of indoor radon concentration and its validation through measurements in South-East Haryana, India. J. Environ. Manage. 171, 35–41. https://doi.org/10.1016/j.jenvman.2016.02.003

Sorokin, V.M., Chmyrev, V.M., Hayakawa, M., 2020. A Review on Electrodynamic Influence of Atmospheric Processes to the Ionosphere. Open J. Earthq. Res. 09, 113–141. https://doi.org/10.4236/ojer.2020.92008

Várhegyi, A., Somlai, J., Sas, Z., 2013. Radon migration model for covering U mine and ore processing tailings. Rom. Reports Phys. 58, 298–310.

Victor, N.J., Siingh, D., Singh, R.P., Singh, R., Kamra, A.K., 2019. Diurnal and seasonal variations of radon (222Rn) and their dependence on soil moisture and vertical stability of the lower

atmosphere at Pune, India. J. Atmos. Solar-Terrestrial Phys. 195, 105118. https://doi.org/10.1016/j.jastp.2019.105118

Warden, S., Bleier, T., Kappler, K., 2019. Long term air ion monitoring in search of pre-earthquake signals. J. Atmos. Solar-Terrestrial Phys. 186, 47–60. https://doi.org/10.1016/j.jastp.2019.01.009

Williams, A.G., Zahorowski, W., Chambers, S., Griffiths, A., Hacker, J.M., Element, A., Werczynski, S., 2011. The vertical distribution of radon in clear and cloudy daytime terrestrial boundary layers. J. Atmos. Sci. 68, 155–174. https://doi.org/10.1175/2010JAS3576.1

Figures

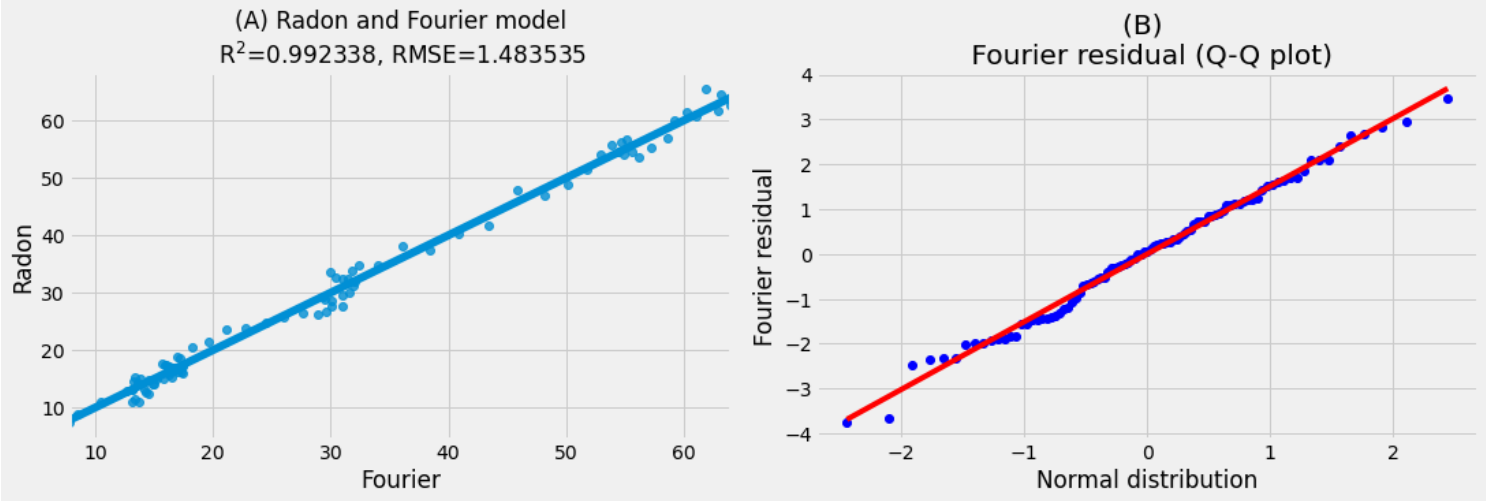

Figure 1

Legend not included with this version

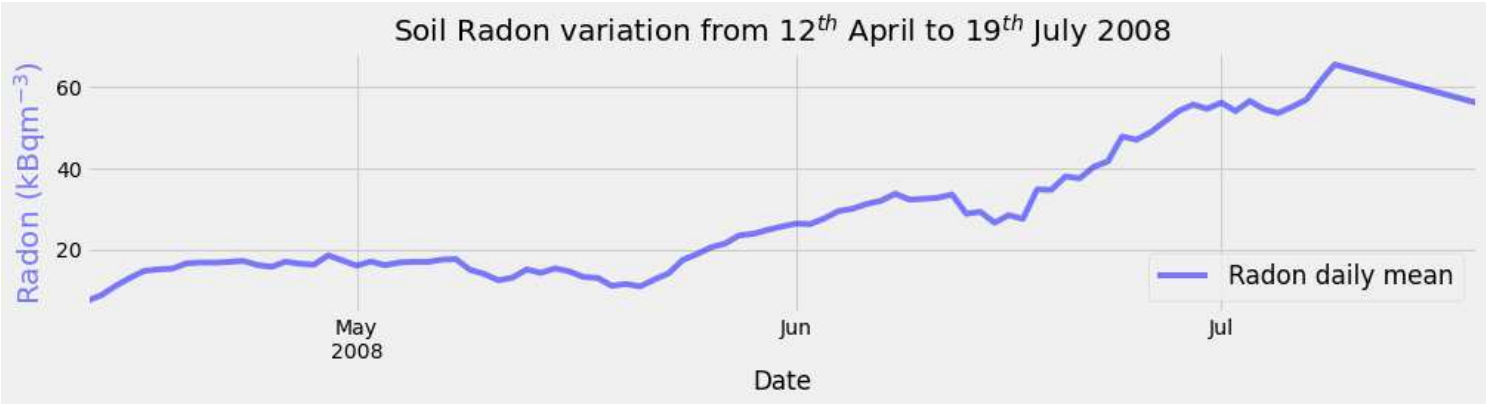

Figure 2

Legend not included with this version

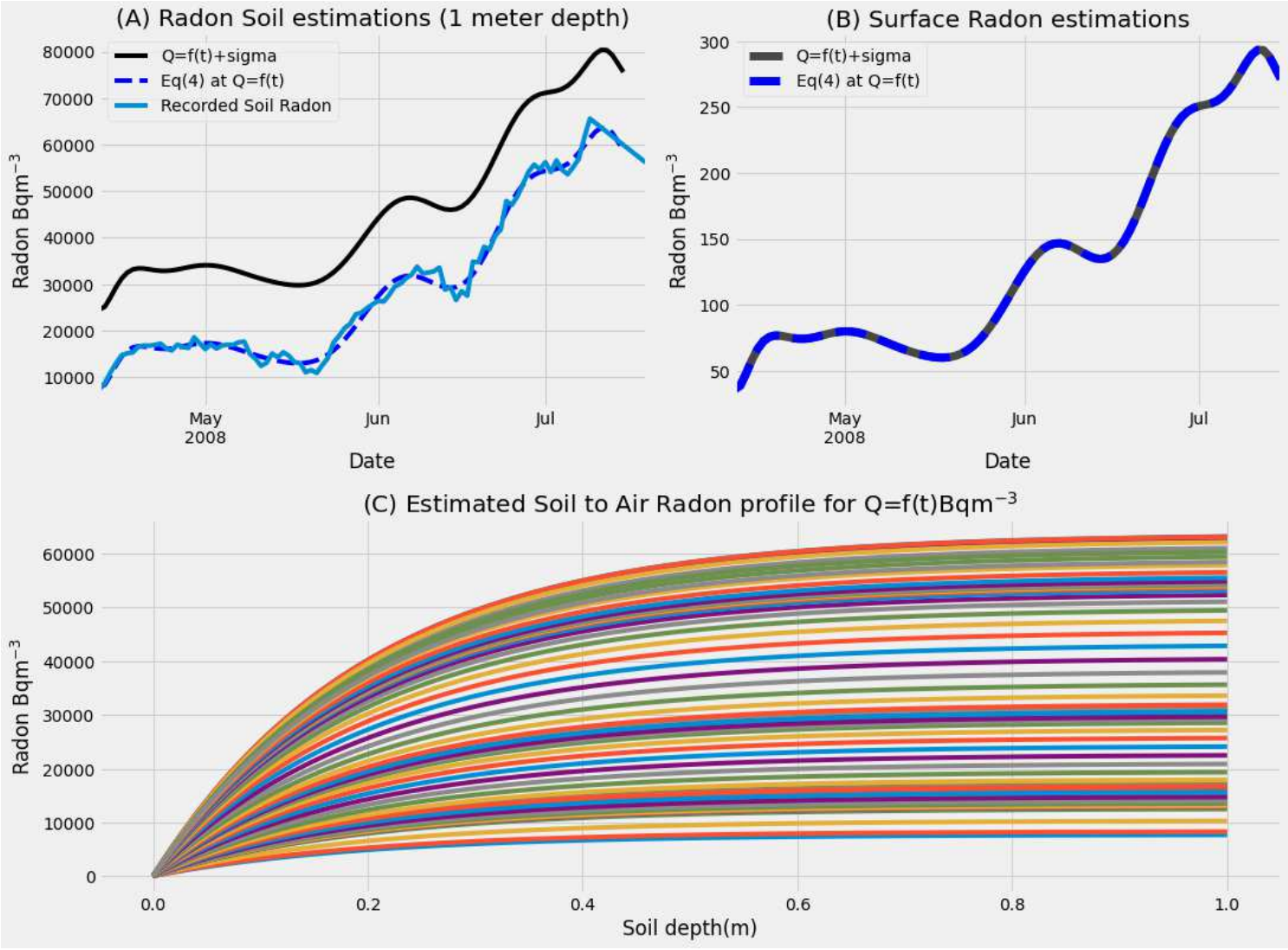

Figure 3

Legend not included with this version

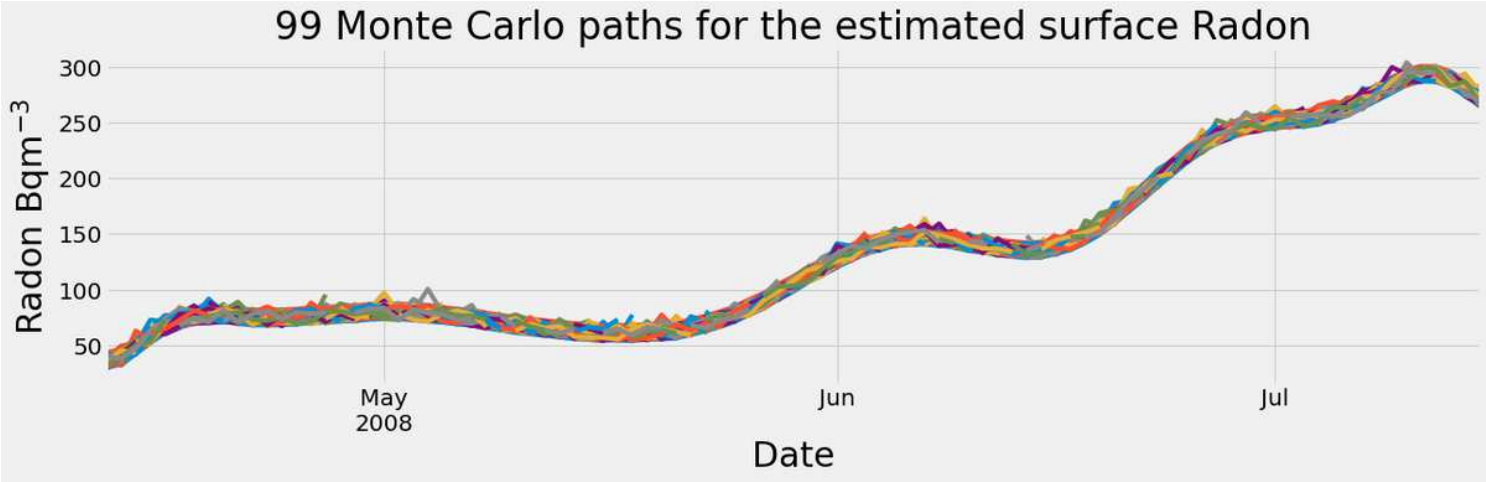

Figure 4

Legend not included with this version

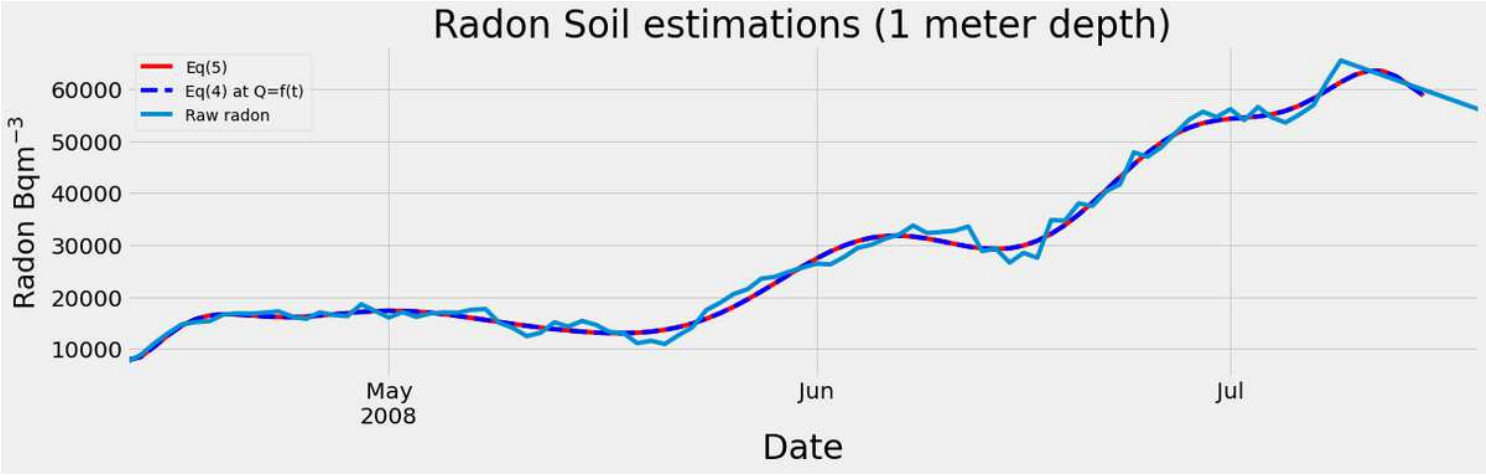

Figure 5

Legend not included with this version

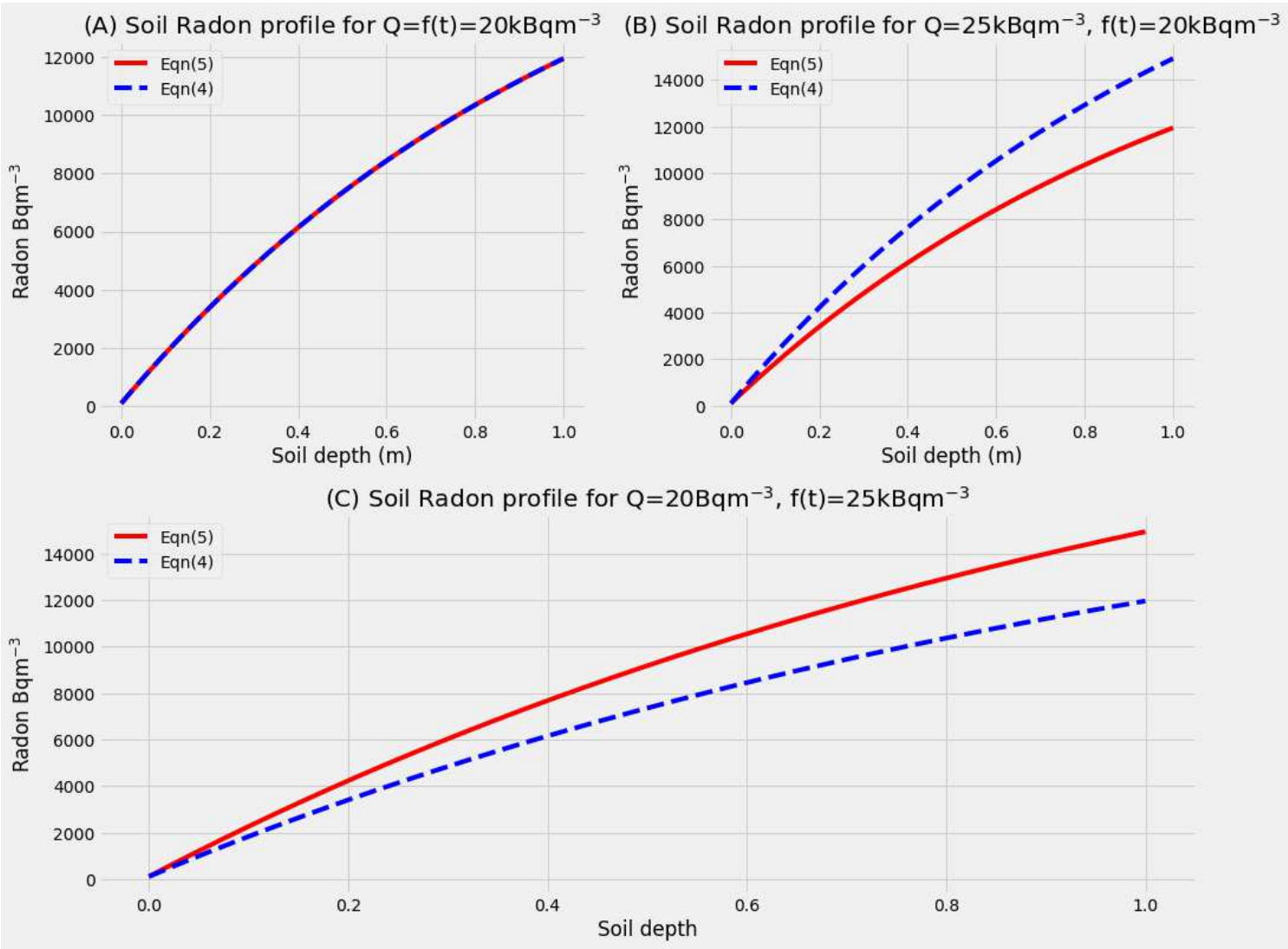

Figure 6

Legend not included with this version